Desalination and Water Treatment
www.deswater.com

doi: 10.5004/dwt.2021.27042

221 (2021) 328–342
May

Complete phenol decomposition from aqueous solutions by electrocoagulation technique using bipolar aluminum configuration

Abeer A. Moneer*, Manal M. El-Sadaawy, Ghada F. El-Said, Fadia A.M. Morsy

National Institute of Oceanography and Fisheries, NIOF, Cairo, Egypt, emails: abeermounir30@gmail.com (A.A. Moneer), manal_dn@yahoo.com (M.M. El-Sadaawy), ghadafarouk25@gmail.com (G.F. El-Said), fadmagd@yahoo.com (F.A.M. Morsy)

Received 13 August 2020; Accepted 15 January 2021

ABSTRACT

Phenol removal was studied with electrocoagulation (EC) technique using bipolar aluminum electrodes. The parameters investigated during the experiment were initial pH, phenol concentration, energy consumption, type of supporting electrolytes, electrodes' number and distance, and current density. The results indicated that phenol molecules were adsorbed on the aluminum hydroxide flocs formed by the anodes, and completely degraded to carbon dioxide and water molecules within just 10 min of different initial concentrations (25–125 mg L^{-1}). The complete decomposition of phenol was confirmed by gas chromatography (GC), scanning electron microscopy, energy-dispersive X-ray spectroscopy, and Fourier-transform infrared spectroscopy techniques. The mechanism of phenol adsorption was described by some adsorption isotherms. Among the adsorption isotherms; Langmuir is the most applicable model, indicating that a monolayer of phenol molecules was formed on the aluminum hydroxide formed on the anode before decomposition. Also, its adsorption mechanism was estimated by kinetic models (pseudo-first-order model, pseudo-second-order model, and intraparticle diffusion). The pseudo-second-order model reflected the dependence of the adsorption process on phenol and aluminum hydroxide concentrations. The computed energy consumption and operating cost confirmed the economic phenol decomposition by EC. A hypothetical equation concerning the complete phenol decomposition was evaluated. Accordingly, it is advisable to use the EC in the removal of phenol for its fast, low energy consumption and total operating cost.

Keywords: Phenol removal; Gas chromatography; Scanning electron microscope; Energy-dispersive X-ray spectroscopy; Fourier-transform infrared spectroscopy; Isotherm models; Kinetic model; Energy consumption; Operating cost

1. Introduction

Recently, considerable interest has been focused on treating polluted water generated from industrial processes. Water pollution due to phenol released from anthropogenic sources such as petrochemicals, oil refineries, coke oven by-products, textile industries, pulp and paper mills, plywood manufacturing, pesticides, insecticides' production units, aircraft maintenance, leather processing units, ceramic plants, pharmaceutical industries, steel plants, dyes, plastics, rubber reclamation plants, mine discharge, explosives, and herbicides have been a major cause of concern for chemists and environmental engineers [1–4]. Besides, there are two natural sources of phenol in the aquatic environment, animal wastes, and decomposition of organic wastes [5]. Phenol compounds are pollutants of paramount importance because they are toxic to aquatic life and human even in low concentrations (5–25 mg L^{-1}), and many of the phenolic compounds have been classified as a hazardous pollutant because of their prospects of harming human health [1]. They can cause anorexia, headache, trouble in gulping, vomiting, sore throat, cerebral pain, fainting, liver and kidney damage, and other mental disorders. The maximum permissible limit of discharged

* Corresponding author.

phenol in wastewater has been set by the Environmental Protection Agency to be less than 1 μg mL^{-1}. In view of the recommendations of World Health Organization, the allowable concentration of phenolic compounds in potable water should not exceed 1 μg L^{-1} [6–8].

In the literature, many techniques such as membrane bioreactors [9], ion exchange resins [10], chemical oxidation [11], chemical coagulation [12], zinc oxide nanoparticle [13], adsorption [14,15], photocatalysis [16,17] were used to remove phenol.

Electrochemical techniques, such as electrocoagulation (EC) are easy to perform, require powerful and compact instrumentation, and use a minimum amount of chemicals. In addition to its other conventional applications, EC is considered as an alternative technology for wastewater treatment. Compared with other conventional techniques, "*in situ*" delivery of reactive agents and no generation of secondary pollution are the most important advantages of EC [18]. In the EC process, the sacrificial electrode is used for the generation of a coagulant agent (usually aluminum and iron hydroxides) that can create flocs for settling and helping to separate water contaminants [7,19]. The following mechanisms describe the reactions that occur when aluminum electrodes are used in EC:

At the anode

$$Al_{(s)} \rightarrow Al^{3+}_{(aq)} + 3e^- \quad (1)$$

$$2H_2O \rightarrow O_2 + 4H^+_{(aq)} + 4e^- \quad (2)$$

At the cathode

$$4H^+_{(aq)} + 4e^- \rightarrow 2H_{2(g)} \quad (3)$$

The formed aluminum ions (Al^{3+}) during the aluminum anode dissolution spontaneously hydrolyze and produce many monomeric, dimeric, trimeric, and polynuclear species that make the anode surrounding the acidic medium. In contrast, the evolution of hydrogen gas makes the cathode area alkali [20]. Also, the aluminum species probably react with OH^- ions to form $Al(OH)_3$ [20]. Accordingly, the mechanism of EC using Al electrodes can be expressed by two parallel steps of charge neutralization and incorporation of impurities in the precipitated $Al(OH)_3$ flocculate in the solution bulk [20]. These two steps are dominantly influenced by pH and aluminum hydroxide mass.

Few studies investigated the removal of phenols using EC technology. Uğurlu et al. [21] studied the removal of phenol by EC using both (Al and Fe) as scarifying electrodes. They found that the Al electrode performs at an efficiency higher than the Fe electrode (98% and 93%, respectively). Also, Kobya et al. [1] investigated the removal of phenol from aqueous solutions by EC using Fe and Al electrodes at the optimum operating conditions with removal efficiencies of 98.6% and 99.2% for Fe and Al electrodes, respectively. While, the performance of phenol removal from aqueous solutions by EC process using also Fe and Al as sacrificial anode with maximum efficiencies of 94.72% and 98.0%, respectively, was recorded by Bazrafshan et al. [2]. On the other hand, phenol removal from aqueous solutions by EC technique was carried out by using only Fe electrodes reaching maximum % removal of 91%. [22]. Zn anode was applied for the first time to remove phenols from wastewaters by Fajardo et al. [23]. They reached maximum removal of only 84.2% at optimum condition (pH of 3.2, a current density of 250 A m^{-2}, electrode distance of 1.0 cm, and 1.5 g L^{-1} of NaCl). Conclusively, Al electrodes always had better efficiencies than any other metals with phenol removal. Accordingly, the complete phenol decomposition to carbon dioxide and water in the solution was not achieved in the literature as it was accomplished in the present investigation, which was confirmed using the different instrumental analyses.

In the present work, the phenol removal from aqueous solution was examined using vertically oriented electrodes made of Al. Several parameters, namely initial pH, initial phenol concentration, type of supporting electrolyte, NaCl concentration as supporting electrolyte, electrodes' distance, number of electrodes were investigated. The phenol removal by its decomposition pathway can be identified by GC-MS, Fourier-transform infrared spectroscopy (FTIR), scanning electron microscopy (SEM), and energy-dispersive X-ray spectroscopy (EDAX). Also, different models of adsorption isotherms, kinetic equations can be used to assess the decomposition mechanism procedure.

2. Materials and methods

2.1. Materials

Phenol (C_6H_5OH) of analytical reagent grade (99.99%, Sigma-Aldrich, Germany) was used for the preparation of synthetic phenol solutions of various initial concentrations (25, 50, 75, 100 and 125 mg L^{-1}). Aluminum (Al) sheets (purity: 95%, product of Egyptian Copper Company, Alexandria, Egypt) performed as sacrificial electrodes. Sodium salts of chloride, sulfate, carbonate, and acetate (products of El Nasr Pharmaceutical Chemicals Company, Egypt) were used as supporting electrolytes. HCl and NaOH (Sigma-Aldrich, Germany) were utilized in the pH adjustment.

2.2. Experimental set-up

The characteristics of the EC reactor are given as described in previous work [24]. Typically, a specific volume of phenol (1 L) was transferred into the cell. After taking the initial sample, the current was then applied under regular magnetic stirring to attain uniform mixing. A trough tube was mounted at the bottom of the cell, with a sampling valve for taking samples of product water at different time intervals. To ensure that the current was direct current (DC), both anode and cathode were connected to the DC power supply. Two devices were connected to the cell (an ammeter and a voltmeter to adjust the current and the potential of the cell).

2.3. Procedure

On performing each experiment and before starting it, the electrodes were subjected to the following steps to avoid the presence of any uncleanness; using abrasive paper

to remove any accumulated particles, washing with distilled water and then immersed in solutions of HCl (35%) and hexamethylenetetramine (2.8%) to get rid of any oxide films formed on the electrode' surfaces [25,26]. Finally, the electrodes' surfaces were rinsed several times with deionized water. For the cell, the cleaning procedure was as follows: the cell was washed with running tap water for about 5 min and then soaked in distilled water for another 5 min; the latter step was triplicated. Phenol solution was poured into the cell after fitting the electrodes in their grooves. The solution in the cell was stirred magnetically, and 5 mL samples of the treated water were withdrawal each 10 min after starting the experiment. The samples were filtered by filter paper 45 μm (Whatman) before analysis, and then the unknown concentration of the filtered samples was evaluated from the calibration curve.

2.4. Phenol determination

Fresh stock solution of phenol as required was prepared daily and was stored in a brown-colored glass reservoir. Before running each experiment, the C_0 was checked. The determination of phenol was carried out using Unico UV-2000 spectrophotometer. The concentration of phenol was determined by the 4-aminoantipyrene method at λ_{max} = 500 nm. [27]. The pH values were measured before and after the removal by the pH meter (model 607). The pH of the electrolyte was adjusted with 1 M HCl or 1 M NaOH. The removal results of different conditions were obtained and analyzed by using % removal of phenol (% Re) as represented in Eq. (4) [28,1]:

$$\%\,\mathrm{Re} = \frac{C_0 - C_t}{C} \times 100 \tag{4}$$

where C_0 and C_t (mg L^{-1}) were the initial and interval time (t) concentrations of phenol. All experiments were performed at 25°C.

2.5. EC equilibrium studies

The amount of phenol adsorbed at equilibrium onto aluminum hydroxide species belonging to the anode, Q_e (mg g^{-1}), was calculated using Eq. (5):

$$Q_e = \frac{C_0 - C_e}{W} \times V \tag{5}$$

where C_0 and C_e (mg L^{-1}) represented the initial and the equilibrium phenol concentrations, respectively. V was the phenol solution volume (L), while W illustrated the aluminum coagulant mass, which can be evaluated from Faraday Law according to the following equation [24]:

$$W = \frac{MIt}{nF} \tag{6}$$

where M, I and t were the molar mass (g mol^{-1}) of the aluminum, amount of current (A), and EC time (s) respectively. While the value of n expressed the number of electrons involved (3 for Al) and F quantified the Faraday's constant (96,485 C Mol^{-1}).

2.6. Instrumental techniques

The functional groups of the adsorbed phenol molecules and formed aluminum hydroxide species by anode electrodes during the EC phenol decomposition process within 7 and 10 min were studied by PLATINUM Diamond ATR accessory and VERTEX 70 FT-IR-Bruker spectrometer. The surface morphology and the elemental composition of the surface anode electrodes, and adsorbed phenol molecules onto formed aluminum hydroxide species were also estimated by SEM and EDAX techniques using Quanta 250 SEM FEI-orbit scientific.

The decomposition of phenol was followed by using Thermo Scientific gas chromatography GC Trace 1300 coupled with an EI Mass spectrometer ISQ 7000 model (Thermo Scientific, USA) equipped with Thermo TR-50 MS capillary column (30 m in length × 250 μm in diameter × 0.25 μm in a thickness of film). Spectroscopic detection by GC–MS involved an electron ionization system that utilized high energy electrons (70 eV), MS transfer line temperature 300°C, and ion source temperature 300°C. Pure helium gas (99.995%) was used as the carrier gas with a flow rate of 1 mL/min. The initial temperature was set at 60°C for 2 min, then increased to 100°C at a rate of 10°C min^{-1} kept for 5 min, then with 10°C min^{-1} to 150°C and kept for 5 min, then with 10°C min^{-1} to 200°C and kept for 5 min, then with 10°C min^{-1} to 250°C and kept for 20 min. For GC-MS phenol analyses, phenol solution was shaken with methylene chloride (Sigma-Aldrich, Germany) and then centrifuged for 10 min at 2,000 rpm. Then the extracted phenol sample was dried by adding traces of sodium sulfate anhydrous salt. Finally, one microliter of the dried extracted phenol sample was injected in a splitless mode to determine its concentration.

3. Results and discussion

3.1. Applied variable conditions

Generally, the % Re of phenol shows significant values ranging from 94.27 to 99.99 after only 10 min in varying conditions of concentration, pH, NaCl dose, electrolyte type, electrodes' number, and electrodes' distance (Fig. 1).

Fig. 1a shows that the high initial concentrations of phenol 100 and 150 mg L^{-1} give almost the same percentage removal (97.93 and 97.99, respectively) within 10 min of EC. These high phenol percentage removals may relate to the remarkable fact that higher the initial concentration, higher the percentage removal, and this is possibly attributed to the presence of sufficient quantities of phenol, which increases the driving force for floc formation and consequently the driving force for phenol removal. Accordingly, it was decided to conduct the following experiments with an optimum initial phenol concentration of 100 mg L^{-1}.

The studied pH range of 2–11 is adjusted to the desired value in each experiment using HCl or NaOH. Obviously, in the present study, the initial pH has a significant effect on the efficiency of phenol removal and its value in the bulk of the solution during the EC process (Fig. 1b).

At initial pH 2, the final pH of the bulk of the solution becomes 4.42, while, at initial pHs 4–11 the final pH reaches pHs 7.75–8.77. This agrees with the documented works, which mentioned that the change in pH depends on the type of electrode material and initial pH [29]. These results show that the removal percentage decreases with the pH increase; however, the higher phenol removal is obtained in an initial pH range of 2–6 due to the formation of the aluminum hydroxide on the anode [20]. Accordingly, the resulting aluminum hydroxide affects the coagulation/co-precipitation

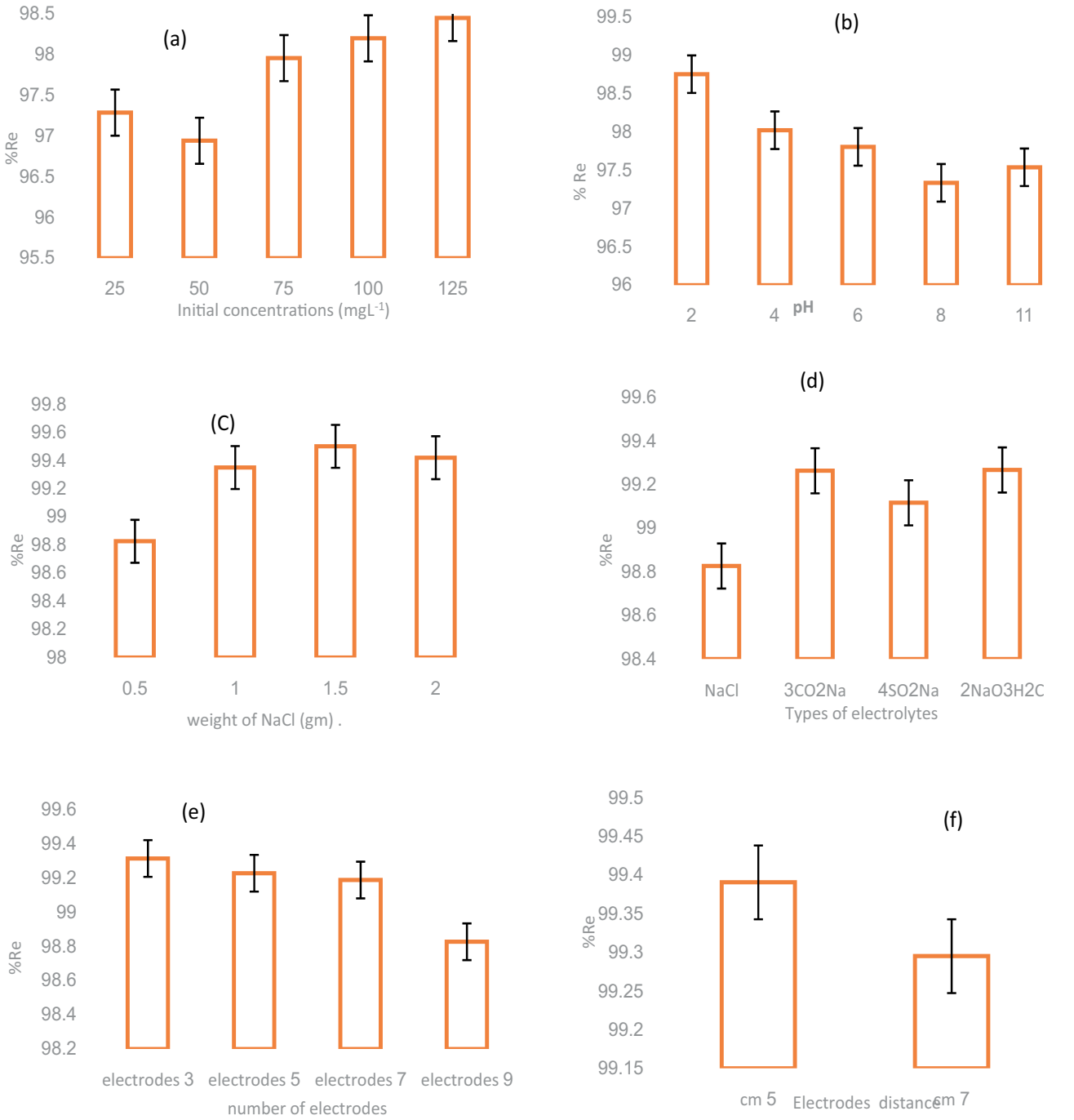

Fig. 1. Effect of different variables on % Re with constant conditions: 1 L, 750 rpm, 25°C, 12 V, 5 A (a) effect of initial concentration, conditions: 9 Al sheets, 0.5 g NaCl, pH = 5.2, (b) effect of pH, conditions: 100 mg L^{-1}, 9 Al sheets, 0.5 g NaCl, (c) effect of weight of NaCl, conditions: 100 mg L^{-1}, 9 Al sheets, pH = 2, (d) effect of type of electrolytes, conditions: 100 mg L^{-1}, 9 Al sheets, pH = 2, 0.5 g of electrolyte, (e) effect of electrodes' number, conditions: 100 mg L^{-1}, pH = 2, 0.5 g NaCl, and (f) effect of electrodes' distance, conditions: 100 mg L^{-1}, 4 Al sheets, pH = 2, 0.5 g NaCl.

of phenol, that is, the adsorption process on the anode [30,31,1]. In contrast, in alkaline initial pH higher than 7, other Al species can be formed such as $[Al(OH)_4^-]$, which is not responsible for the phenol removal for the fact that it is soluble and impractical for adsorption of phenol [32].

The supporting electrolytes play a vital role in the EC process due to the possibility of the formation of side products that can affect the efficiency of the system. NaCl was used as an electrolyte at different concentrations (0.5, 1, 1.5, and 2 g L^{-1}) to investigate its effect on the phenol removal during the EC process at optimum operational conditions of 100 mg L^{-1}, 1 L, 9 Al sheets, 750 rpm, 25°C, 12 V, 5 A, and pH = 2 (Fig. 1c). The various NaCl concentrations give relatively similar high phenol removals 98.7%, 99.66%, 99.91%, and 99.83%, respectively. This indicates that the increase of NaCl dose as a supporting electrolyte is not worth. Whereas, the relatively similar percentage removal of phenol is related to the increase of the solution electric resistance that affects negatively the efficiency of the process. Because this fact is attributed to the competitive effect of both Cl^- and phenol with the formed $Al(OH)_3$; especially in high sodium chloride dosage, in addition to the reduction in the speed of the ions as a result of the retardation force of the inter-ionic attraction [33,34].

It is noteworthy that using different types of supporting electrolytes such as sodium carbonate, sodium sulfate, and sodium acetate leads to almost the same % Re of phenol with an extremely narrow difference (Fig. 1d), which suggests that using the supporting electrolyte for phenol removal is simply for improving the electric conductivity in the EC cell without any possible interference with the cell chemical reaction or the adsorption process of phenol and its degradation.

In experimental work, the increase in the number of Al electrodes from 3 to 9 gives significant phenol removal (Fig. 1e). This very high removal is probably related to the complete decomposition of phenol at anode within only 10 min of EC progress. However, the increase in the Al electrode number leads to an increase in the surface area that hence generates more coagulants in the EC process [35]. Besides, the increase in the electrode number generates greater amounts of aluminum hydroxide polymers with slower movements that tend rather to aggregate and adsorb the phenol molecules than being attracted to the electrode surface. In the present work, using three electrodes can accomplish the mission and it is also more economical to use the minimum number of electrodes as long as the process can be completed with the same efficiency.

The possible effect of electrodes' distance is investigated by changing the distance between two middle electrodes in addition to the cathode and anode. The variation of the spacing between the electrodes from 5 to 7 cm indicates that the increase in spacing between the electrodes decreases the removal efficiency of phenol during the EC progress (Fig. 1f). The presented data are in good agreement with those previously studied. However, the increase in spacing between electrodes leads to less interaction between phenol molecules and hydroxyl polymers and thus increases the chance of Al hydroxides to coagulate to form the flocs [36]. Plus, the decreasing distances between cathodes and anodes lower the required electrical energy for the motion of ions, that is, reduce the resistance of ions during their motion path and vice versa for the large distance [37].

3.2. Characterization of electrodes and flocs during EC process

The phenol decomposition mechanism was studied within 7 and 10 min of the EC process by analyzing the formed adsorbed aluminum hydroxide species formed by anodes and flocs with FTIR, SEM, EDAX techniques. The decomposition of phenol in the bulk of the solution during the EC process was followed by GC-MS technique. The remarkable efficiency of phenol decomposition is followed by SEM, EDAX, FTIR, and GC-MS techniques in a chosen time (7 min) and in the decomposition time (10 min) (Figs. 2–6).

An EDAX image of aluminum anode represents the purity of it at the beginning of the EC experiment (Fig. 2a). Whereas the EDAX images for Al anode and the formed flocs in 10 min show the presence of the formed aluminum hydroxide, and the disappearance of phenol; that is, they confirm the complete phenol degradation in only 10 min of EC progress (Figs. 2b and c). These results go in harmony with the previous studies dealing with the complete phenol decomposition into carbon dioxide gas and water at the end of the electrolysis experiment [38,39].

The performance of SEM describes the uniform surface of the aluminum electrode at the beginning the EC process (Fig. 3a). Fig. 3b shows the formation of a rugged surface including some dents at the completeness of the EC process. Plus, this figure confirms the unique formation of the polymer Al hydroxide species at the anode surface at the ultimate of the experiment due to the dissolution of it and the release of oxygen gas [40].

FTIR spectrum of the formed aluminum hydroxides at the anode and the flocs in the bulk at the end of the EC procedure, also, agrees with the results of both SEM and EDAX analyses (Fig. 4). However, this spectrum for the ultimate of the EC experiment also assures the complete decomposition of the adsorbed phenol molecules on the formed aluminum hydroxide polymers at the anode and the absence of phenol molecules in the Al hydroxide flocs. Fig. 4 gives bands 3,366 and 3,287 cm^{-1}, respectively, corresponding to the stretching vibration of OH [41]. Peaks 1,642 and 1,643 cm^{-1} related to OH bending in the hydration of water [42]. Additionally, the peaks of 1,571; 1,519; 1,423; and 1,392 cm^{-1} for anode and 1,509; 1,390; and 1,057 cm^{-1} for flocs reflect the formation of $Al(OH)_3$ [41]. However, it was reported that the band between 1,800 and 1,300 cm^{-1} with a maximum of 1,510 cm^{-1} accompanied with OH group and spectrum between 1,100 and 200 cm^{-1} referred to $Al(OH)_3$ [41]. The polymeric species of Al are assigned in 1,392 and 1,390 cm^{-1} for anode and flocs, respectively [42]. A band of 974 cm^{-1} in the spectrum of anode corresponds to the bending vibrations bonds Al–OH and Al–O–Al, whereas, the peaks at 522 cm^{-1} may relate to octahedral coordination of AlO_6 [42].

Interestingly, the FTIR for the formed aluminum hydroxide species at the anode in 7 min of the EC process emphasizes the step of the adsorption of the phenol molecules on the $Al(OH)_3$ species at the anode (Fig. 5). However, in FTIR, 3,339 cm^{-1} is assigned for the OH stretching and

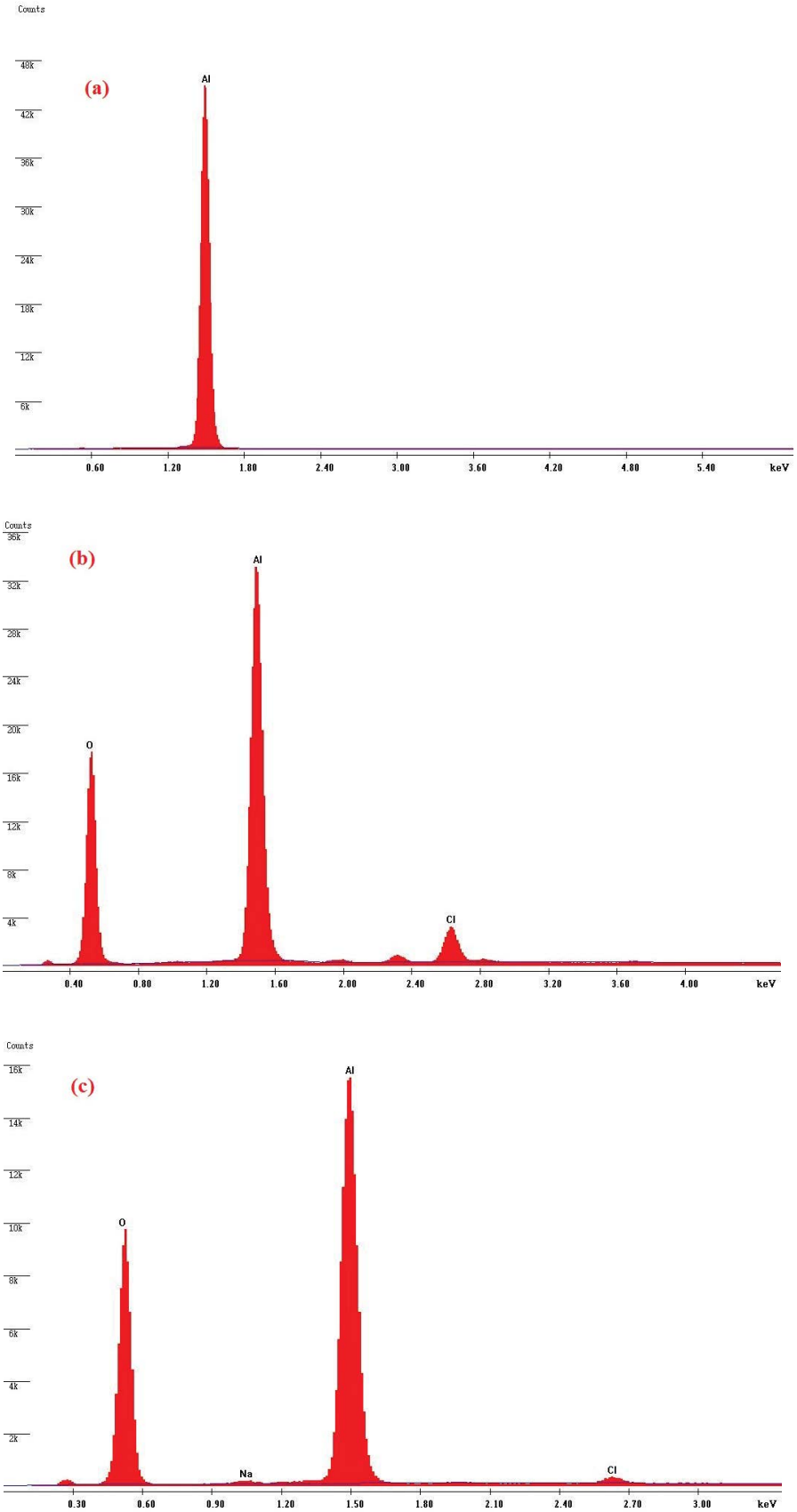

Fig. 2. EDAX images EC process: (a) anode at the beginning of EC, (b) anode after 10 min, and (c) the formed flocs after 10 min.

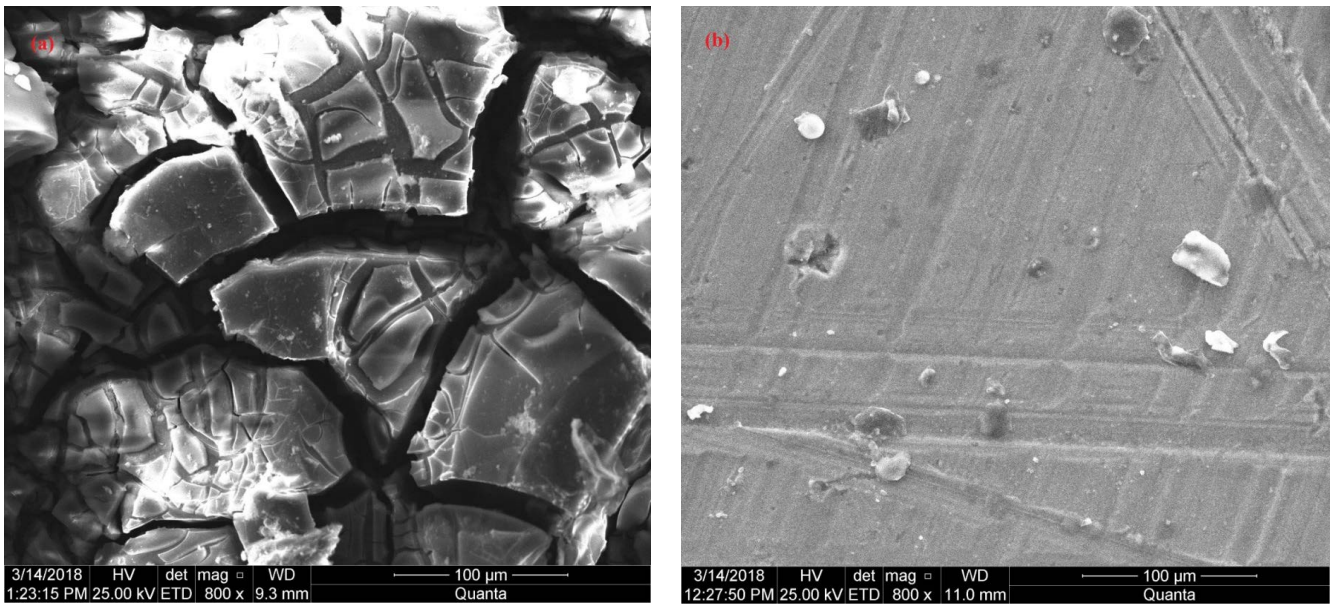

Fig. 3. Scanning electron microscopy images EC process: (a) anode at the beginning of EC and (b) anode after 10 min of EC progress.

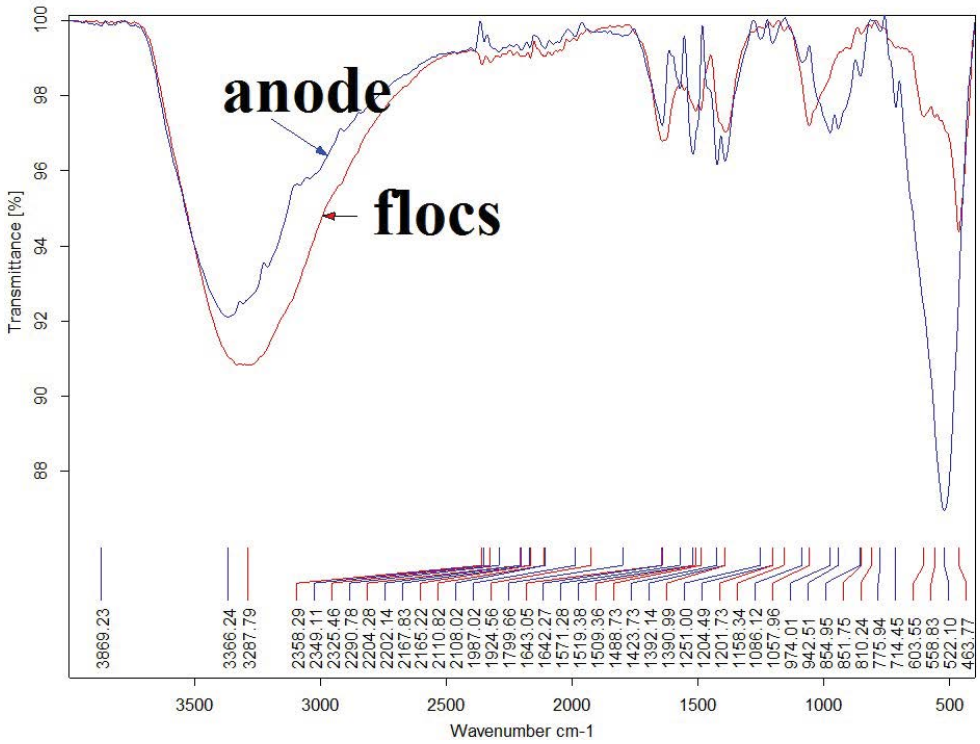

Fig. 4. Fourier-transform infrared spectroscopy images for anode and flocs after 10 min EC progress.

the notable peak in 507 cm^{-1} relates to the Al species [42]. Whereas, 1,633 and 970 cm^{-1} are corresponding to C=C of the aromatic phenol ring [31,38].

The GC–MS analysis of the bulk of the solution of 100 µg mL^{-1} phenol in a 7 min of EC process confirms the presence of only 36.29 µg mL^{-1} phenol, that is, about 63.71% of phenol was completely decomposed within this processing period (Fig. 6). This result affirms the fast-total degradation of phenol into carbon dioxide gas and water in one step by EC process during only 10 min of operation under the previously mentioned experimental conditions, which make it the fastest applicable technique for the removal of phenol wastes. Many previous studies concerning the degradation of phenol focused on its complete breakdown

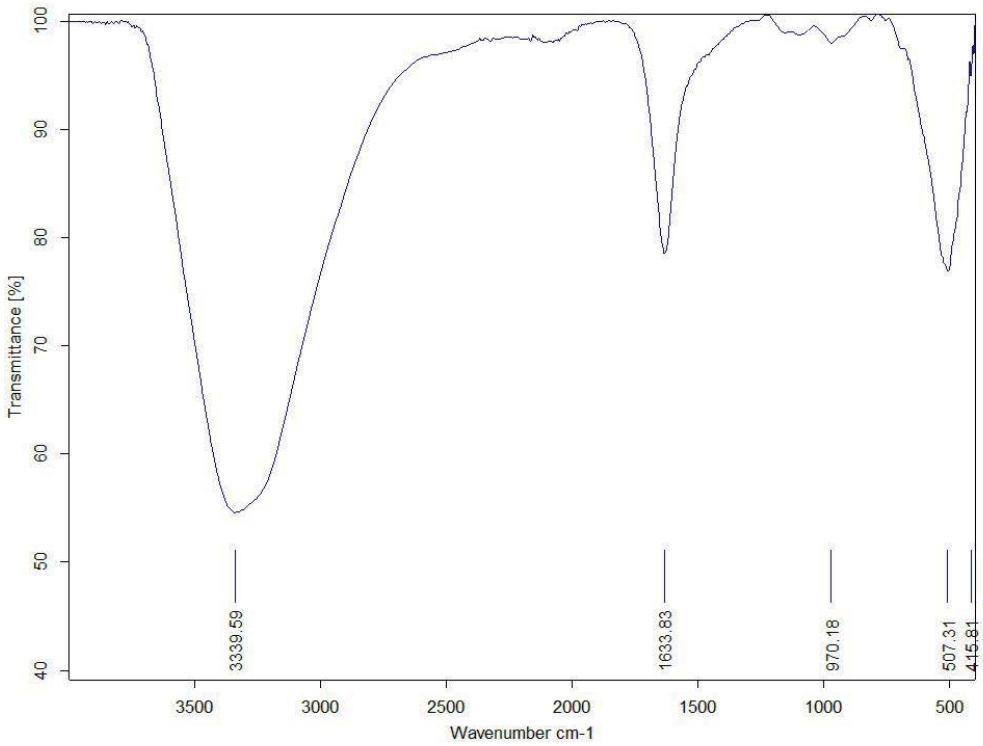

Fig. 5. Fourier-transform infrared spectroscopy image for anode after 7 min of EC progress.

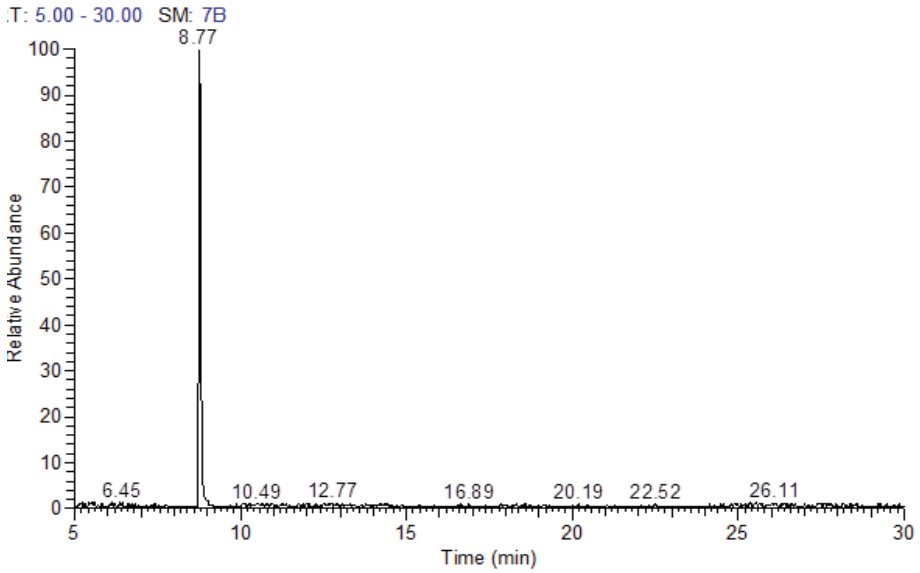

Fig. 6. GC-MS image for anode after 7 min of EC progress.

in many steps including intermediate compounds and in longer proceeding time [1,30,31,38,43].

3.3. Predicted phenol decomposition mechanism

Owing to the formerly used techniques mentioned in the previous section, the decomposition of phenol can be performed in two steps (Fig. 7). The first step is the most critical step, which belongs to the adsorption of phenol molecules on the formed aluminum hydroxide species at the anode. This effective step was previously documented and called by sweep flocs [1]. The second of the proposed mechanism is the complete degradation of phenol into carbon dioxide gas and water. In this published study, the authors decided to follow up the phenol's adsorption mechanism by using various adsorption isotherms and kinetic models.

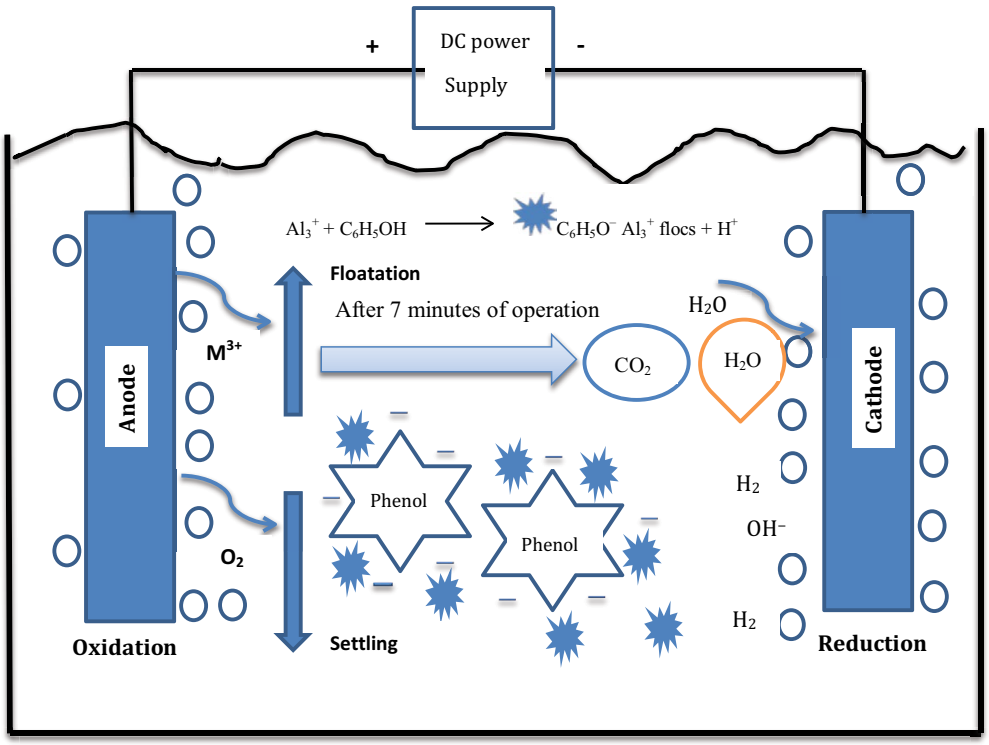

Fig. 7. Mechanism of phenol decomposition by EC process.

3.4. Adsorption isotherms models

The adsorption of phenol on the formed aluminum hydroxide species at the anode during 10 min of the EC process was studied by Langmuir, Freundlich, Temkin, Dubinin–Radushkevich (D-R), and Flory and Huggins (F-H) models. The most fitted isotherm amongst these adsorption models can refer to the most applicable adsorption mechanism. The linear forms of these models are given in Eqs. (7)–(17).

3.4.1. Langmuir isotherm

This adsorption model has been developed for the purpose of explaining the chemisorption phenomenon that can occur at different adsorption sites with the same adsorption energy, far from the surface coverage, and without contact between adsorbed molecules. Langmuir model also assumes a monolayer deposition of the adsorbent on the surface of adsorbate with a limited number of identical sites [44]. The linearized form of Langmuir adsorption isotherm is expressed in Eq. (7) [45].

$$\frac{1}{q_e} = \left[\frac{1}{K_L Q_m}\right]\frac{1}{C_e} + \frac{1}{Q_m} \tag{7}$$

where q_e (mg g^{-1}) is the amount adsorbed at equilibrium concentration C_e (mg L^{-1}), q_m (mg g^{-1}) is the Langmuir constant that represents maximum monolayer adsorption capacity and K_a (L mg^{-1}) is the Langmuir constant related to energy of adsorption. Whereas, the characterization of Langmuir isotherm is expressed by the following equation, which contains the dimensionless constant separation factor or equilibrium parameter (R_L; Eq. (8)):

$$R_L = \frac{1}{1 + K_L C_0} \tag{8}$$

where C_0 represents the initial concentration (mg L^{-1}). As shown in Table 1, the value of R_L is less than unity indicating that the phenol adsorption onto aluminum hydroxide flocs is spontaneous and favorable during the first 10 min of EC processing [46]. The plots of $1/q_e$ as a function of $1/C_e$ for the adsorption of phenol on $Al(OH)_3$ at different initial concentrations are performed. The plots are found to be linear with good correlation coefficients (0.927) indicating the applicability of the Langmuir model in the present study. The values of monolayer capacity (Q_m) and the Langmuir constant (K_a) are presented in Table 1. The small value of Q_m indicating the fast decomposition of phenol by EC.

3.4.2. Freundlich isotherm

This isotherm model typically fits the experimental data over a wide range of concentrations. This empirical model includes considerations of surface heterogeneity and an exponential distribution of the active sites and their energies. The isotherm is adopted to describe reversible adsorption and is not limited to the formation of a monolayer [47].

The linearized logarithmic form of the Freundlich model can be expressed as in Eq. (9) [48]:

Table 1
Constant values of the studied linear adsorption isotherm models for the adsorbed phenol on the aluminum hydroxide species at anode during 10 min EC proceeding

Isotherm models	Isotherm value
Langmuir	
Q_m (mg g^{-1})	2.848
K_a (L mg^{-1})	0.012
R_L	0.003
R^2	0.927
Freundlich	
K_f(mg g^{-1}) (L mg)$^{-1/n}$	0.666
n_f	3.301
R^2	0.855
D-R	
q_m (mol g^{-1})	3.284
E (kJ mol^{-1})	6.74E-04
R^2	0.866
Temkin	
A_T (L g^{-1})	1.270
b_T (kJ mol^{-1})	4.411
R^2	0.732
F-H	
$K_{F\text{-}H}$ (L g^{-1})	1.711
n_{FH}	0.367
$\Delta G°$ (kJ mol^{-1})	–1.330
R^2	0.675

$$\ln q_e = \ln K_f + \frac{1}{n_f}\ln C_e \tag{9}$$

In this equation, K_f is the adsorption capacity. K_f (mg g^{-1}) (L mg)$^{-1/n}$, and n_f is the adsorption intensity. The obtained n_f value is in the range of 1–10 indicates favorability of phenol adsorption [49] (Table 1).

3.4.3. Dubinin-Radushkevich (D-R)

It is generally applied to express the adsorption mechanism by distributing Gaussian energy distribution over a heterogeneous surface, and this model is represented by Eq. (10) [50,51]:

$$\ln q_e = \ln q_m - K_{DR}\varepsilon^2 \tag{10}$$

where q_m is the theoretical saturation capacity (mol g^{-1}), K_{DR} is a constant related to the mean free energy of adsorption (mol^2 kJ^{-2}) and ε is Polanyi potential, which can be calculated by the following equation (Eq. (11)):

$$\varepsilon = RT\ln\left(1+\frac{1}{C_e}\right) \tag{11}$$

where R is the gas constant (8.314 J mol^{-1} K^{-1}); T is the absolute temperature (K).

Furthermore, the mean free energy of adsorption (E) can be illustrated as follows [51]:

$$E = -\left(2k\right)^{-0.5} \tag{12}$$

The E gives information about the type of adsorption. If the E value is less than 8 kJ mol^{-1} then the physical adsorption will occur; on the other hand, the E value is between 8 and 16 kJ mol^{-1} ion-exchange processes will take place, while E values more than 16 kJ mol^{-1} indicates chemical adsorption [52]. As shown in Table 1, the calculated E value (6.74E-04 kJ mol^{-1}) suggests the physical adsorption feature of phenol adsorption on the aluminum hydroxide species at the anode in EC procedure [51,52] (Table 1).

3.4.4. Temkin isotherm

This model deduces the linear inverse relationship between the heat of adsorption and the surface covering according to the sorbent–adsorbate interactions [53]. The linear equation of this isotherm is represented in Eq. (13):

$$q_e = B_T \ln A_T + B_T \ln C_e \tag{13}$$

$$B_T = \frac{\left(RT\right)}{b_T} \tag{14}$$

where A_T: Temkin equilibrium constant related to the binding energy (L g^{-1}), b_T: the equilibrium constant related to the heat of adsorption, T: the absolute temperature in Kelvin, R: the universal gas constant (8.314 J mol^{-1} K^{-1}).

The calculated parameters of Temkin isotherm model A_T and b_T are demonstrated (Table 1). The bonding factor (b_T) assumes the nature of adsorption, b_T < 8 kJ mol^{-1}, the adsorption is of physical in nature and b > 8 kJ mol^{-1} implies the chemical adsorption between the molecules of sorbents and sorbates. In the present study, the value of b_T obtained from this isotherm model (<8 kJ mol^{-1}) suggesting the physical nature of phenol removal by EC [54].

3.4.5. Flory–Huggins (F-H)

Flory–Huggins isotherm explains the degree of surface coverage of adsorbate on the adsorbent isotherm [55]. Its linear form is given in Eq. (15) as follows:

$$\log\frac{\theta}{C_e} = \log K_{FH} + n_{FH}\log\left(1-\theta\right) \tag{15}$$

where θ: the degree of surface coverage, K_{FH} and n_{FH} are an indication of the equilibrium constant and model exponent.

The degree of surface coverage (θ) can be calculated as follows (Eq. (16)):

$$\theta = 1 - \frac{C_e}{C_0} \tag{16}$$

The spontaneous free Gibbs energy ($\Delta G°$) can be evaluated as given in Eq. (17):

$$\Delta G° = -RT \ln K_{FH} \tag{17}$$

K_{FH} is the Flory–Huggins constant (L mol^{-1}) predicts the spontaneity of the adsorption process and the negative value of $\Delta G°$ confirms the applicability and spontaneous feature of phenol adsorption (Table 1) [46].

On the basis of correlation coefficient (R^2), the studied isotherm models could be arranged in decreasing order of favored adsorption isotherm as follows: Langmuir > Dubinin–Radushkevich > Freundlich > Temkin > Flory–Huggins (Table 1).

3.5. Kinetic models

To understand the adsorption behavior of phenol on the aluminum hydroxide species during the first 10 min of the EC procedure, pseudo-first-order, pseudo-second-order, and intraparticle diffusion models are applied. Kinetic models are useful to predict the time needed for adsorption and the rate of target adsorbent uptake and also to describe the adsorption process.

3.5.1. Pseudo-first-order model

The first order Lagergren model is expressed as follows (Eq. (18)) [50]:

$$\frac{dq_t}{dt} = k_1\left(q_e - q_t\right) \tag{18}$$

where q_e and q_t are the adsorption capacities (mg g^{-1}) of phenol at equilibrium and at time t (min), respectively, and k_1 is the equilibrium rate constant of the pseudo-first-order adsorption (min^{-1}) [50].

The integrated form of the above equation with the boundary conditions $t = 0$ to $t = t$ and $q_t = 0$ to $q_t = q_t$ is rearranged to obtain the following time dependency function (Eq. (19)).

$$\ln\left(q_e - q_t\right) = \ln q_e - K_1 t \tag{19}$$

3.5.2. Pseudo-second-order model

The Lagergren second-order kinetic model is expressed as Eq. (20) [50] as follows:

$$\frac{dq_t}{dt} = K_2\left(q_e - q_t\right)^2 \tag{20}$$

where K_2 (g mg^{-1} min^{-1}) is the rate constant of second-order adsorption model. Using the slope and intercept values obtained from a plot of t/q_t vs. t for, the values of K_2 and q_e are computed.

The integrated form of (Eq. (20)) with the boundary condition $t = 0$ to $t = t$ and $q_t = 0$ to $q_t = q_t$ is:

$$\frac{t}{q_t} = \frac{1}{K_2 q_e^2} + \frac{t}{q_e} \tag{21}$$

3.5.3. Intraparticle diffusion model

Both mentioned above Eqs. (18) and (20) cannot give the definite kinetic mechanism of phenol adsorption. A graphical method has been introduced [56] to predict the involvement of the multi-step mechanism in the removal process, also to ascertain whether pore diffusion or intraparticle diffusion is the rate-limiting step. Thus, the intraparticle diffusion model is applied by following the below-given formula [52]:

$$q_t = k_{dif} t^{1/2} + C \tag{22}$$

where k_{dif} represents the intraparticle diffusion rate constant (mg g^{-1} min$^{-1/2}$), and C is the intraparticle diffusion constant (mg g^{-1}). The constants k_{dif} and C can be obtained, from the slope and intercept of the plot of q_t vs. $t^{1/2}$, respectively; however, C is related to the boundary layer thickness of the adsorbed phenol. The R^2 values of the performed kinetic models corresponding to the adsorption of phenol on the aluminum hydroxides in the first 10 min of EC processing reflected that the pseudo-second-order kinetics model is the most applicable model (Table 2), which depends on phenol and aluminum hydroxides' concentrations.

4. Energy consumption

The intended target of the EC technique in common is to handle the extraordinary chemical concentration to a certain acceptable limit without using external chemicals and with low-cost energy consumption. Like so, specific energy consumption in EC treatment along the best phenol removal's optimum operating conditions should be taken into consideration. In the present study, the applied potential differences are measured using a voltmeter at two different current densities of 43.4 and 104.2 A m^2. The specific energy consumption values are calculated according to Eq. (23) [57,58]:

$$\text{Energy Consumption}\left(\text{kWh/kg}\right) = \frac{I \times v \times t}{\left(C_0 - C_t\right) \times V} \tag{23}$$

Table 2
Parameters values of the used kinetic models for the adsorption of phenol the adsorbed phenol on the aluminum hydroxide species at anode during 10 min EC proceeding

Kinetics model	Parameters and regression coefficient	Value
Pseudo-first-order	K_1 (min^{-1})	0.03
	R^2	0.477
Pseudo-second-order	K_2 (g mg^{-1} min^{-1})	0.11
	R^2	0.990
Intraparticle diffusion	K_{dif} (mg g^{-1} min$^{1/2}$)	2.12
	C (mg g^{-1})	175.93
	R^2	0.876

where I is current density (A), v is applied potential difference (Volt), t is reaction time (h) and V is the volume of solution (m^3).

Fig. 8 illustrates that the energy consumption is much higher in the case of using a current density of 104.2 A m^2 while inspecting (Fig. 8) indicates that using this higher current density does not cause a great difference in percentage removal under optimum conditions stated in the figure caption but also gave lower percentage removal in some cases. Especially, with the optimum phenol concentration studied in the present work (100 mg L^{-1}) and as it can be seen from (Fig. 9), the percentage removal was almost the same for the two current densities used. Consequently, it was decided for power saving sake that using the current density of 43.4 A m^2 is more economical.

5. Total operating cost (TOC)

The TOC (US$/$m^3$) of the decomposition of phenol during 10 min of EC processing is calculated using the specific energy consumption (EC) and cost of the aluminum electrode (ELC) in the given Eqs. (24) and (25) [59]:

$$\mathrm{ELC} = \frac{I \times M_w \times t_{\mathrm{EC}}}{n \times F \times V} \tag{24}$$

$$\mathrm{TOC} = £\mathrm{EC} + \beta\mathrm{ELC} \tag{25}$$

where F is the Faraday's constant (96.487 C mol^{-1}), n represents the number of transferred electrons (3 electrons) for aluminum, V is the volume of solution (m^3), t_{EC} operating time of EC (h) and M_w (kg mol^{-1}) is the molecular mass of aluminum.

The prices of the electrical energy for industrial sector £ and aluminum electrodes ß in the Egyptian market during June 2019 were 0.05 US$/1 kWh and 0.55 US$/1 m^3, respectively. The results show that the TOC (US$/$m^3$) of phenol decomposition is 0.75 US$/$m^3$. This value is lesser than those previously reported for EC techniques for the removal of phenol (6.1 €/m^3) [1]. This indicates the economic importance of the EC technique application in the complete decomposition of phenol.

6. Statistical presentation

The correlation matrix of % Re of phenol, the experimental conditions of EC processing time, initial phenol concentration, initial pH, number of electrodes, amount of NaCl, current density, potential differences, and Al consumption are achieved by using IBM SPSS STATISTICA 22 program at significant level $p < 0.05$. It almost gives high significant correlation coefficients among all experimental variables (Table 3). This confirms the effectiveness of these variables on the phenol removal by EC procedure.

A multiple regression hypothetical equation for the percentage removal of phenol as dependant variable under various independent variables of initial pH, EC processing time (min), initial phenol concentration (mg L^{-1}), amount of NaCl (g), number of electrodes, current density (A), potential differences (Volt) and aluminum consumption (g) at constant values of temperature (25°C ± 2°C), stirring speed and bulk volume (1 L) using STATISTICA 22 program is performed (Table 4). From the resultant multiple regression report concerning the high significant predicted equation (R = 0.8983), the hypothetical equation can be illustrated as shown in Eq. (26):

$$\%\,\mathrm{Re} = 96.92 + 0.20\,\mathrm{Time} + 0.60\,C_{\mathrm{initial}} - 0.29\,\mathrm{pH} - 0.18\,\text{electrode's number} + 0.21\,\mathrm{NaCl} - 0.10\,\mathrm{Al\ consumption} \tag{26}$$

The graphical comparison between the experimental results and the predicted data confirm that this equation

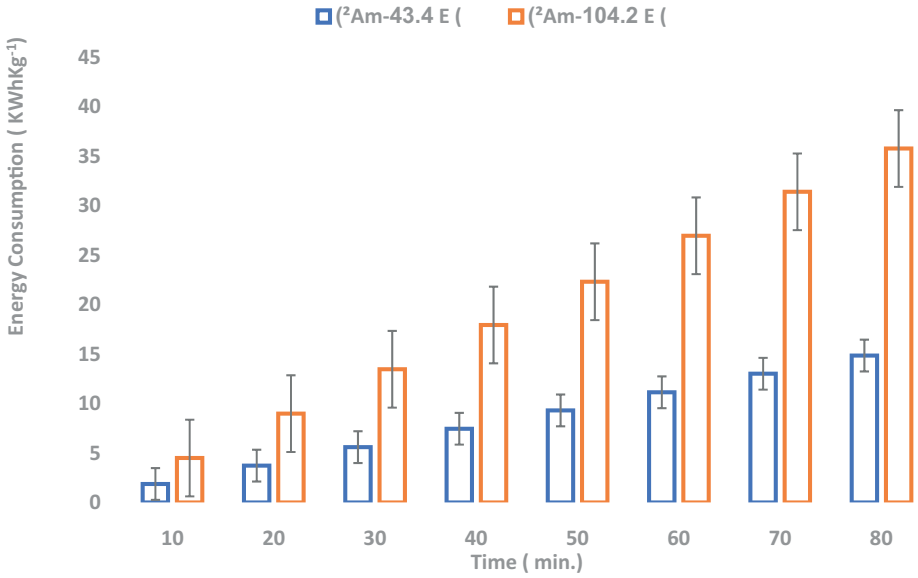

Fig. 8. Energy consumption of EC for phenol decomposition using two current densities in 10 min of EC progress (750 rpm, 25°C, pH = 2, initial concentration (100 mg L^{-1}), 9 Al electrodes).

Table 3
Correlation matrix among % Re and other experimental variable conditions ($p < 0.05$)

Variable	Time	$C_{initial}$	% Re	pH	No. electrodes	NaCl	Current	Potential difference	AL consumption
Time	1.000								
$C_{initial}$	0.019	1.000							
% Re	0.093	0.759	1.000						
pH	0.147	–0.294	–0.596	1.000					
No. electrodes	–0.003	–0.144	–0.346	0.325	1.000				
NaCl	–0.009	0.136	0.371	–0.304	0.119	1.000			
Current	0.004	–0.293	–0.478	0.405	0.188	–0.177	1.000		
Potential difference	0.004	–0.293	–0.478	0.405	0.188	–0.177	1.000	1.000	
AL consumption	0.720	–0.170	–0.213	0.370	0.115	–0.114	0.619	0.619	1.000

Table 4
Resultant multiple regression report of the high significant predicted equation ($R = 0.89829747$, $p < 0.0000$, $n = 206$)

Independent variable	Beta	SE. Beta	B	SE. B	*T*	*p*-level
Intercept			96.92	0.30	324.07	0.00E+00
Time	0.20	0.05	0.01	0.00	4.30	2.72E-05
$C_{initial}$	0.60	0.03	0.03	0.00	17.99	1.33E-43
pH	0.29	0.04	–0.14	0.02	–7.49	2.26E-12
Electrode number	0.18	0.03	–0.15	0.03	–5.27	3.58E-07
NaCl	0.21	0.03	0.80	0.13	6.34	1.54E-09
Aluminum consumption	0.10	0.05	–0.10	0.05	–2.10	3.74E-02

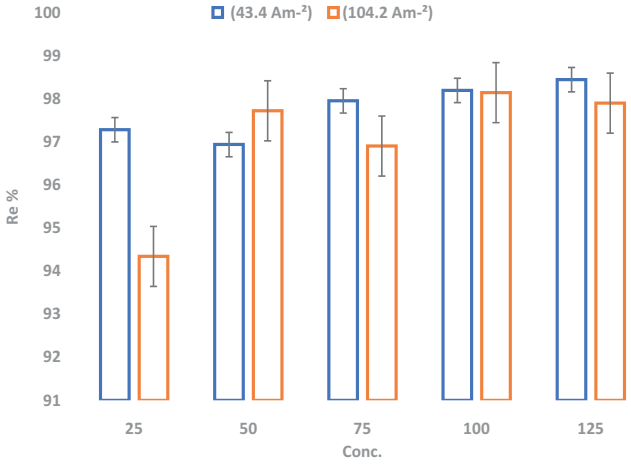

Fig. 9. Removal percent for various phenol concentrations (25–125 mg L^{-1}) of two current densities in 10 min of EC progress.

can be applied as a hypothetical phenol removal equation under the presented experimental condition (Fig. 10).

7. Conclusion

The complete decomposition of phenol from its solutions by using the aluminum bipolar EC technique was examined by different instrumental measurements. The effect of initial phenol concentration, type and quantity of supporting electrolyte, initial pH, current density, potential differences, aluminum consumption, electrode's distance, and number was investigated to obtain the most optimum removal conditions using the EC operation. It was concluded that for most of the conditions, the percentage removal of 100 mg L^{-1} initial concentration of phenol was in the range of 94%–99%. A pH of 2 was optimum and 0.5 g of NaCl as supporting electrolyte was chosen. Also, it was concluded that the number and electrode distance factors were not of prime importance in the present work. The phenol removal was studied by correlation matrix and multiple regression statistical analyses. These statistical methods confirmed the high significant phenol removal under the used experimental conditions. The multiple regression performance produced a significant hypothetical phenol removal equation. The instrument measurements of SEM, EDAX, FTIR, and GC-MS confirm that the complete removal of phenol was performed by two steps within only 10 min. The first step belonged to its adsorption on the formed aluminum hydroxide species at the anode surface, thus the adsorption and the kinetics of this process could be studied. And the mechanism of this aforementioned step was studied by some isotherms and the kinetic models. The adsorption mechanism of phenol on the aluminum hydroxide species was studied by using Langmuir, Freundlich, Dubinin–Radushkevich (D-R), Temkin, and Flory and Huggins (F-H) isotherm models. The results reflected that the Langmuir model was the most applicable isotherm

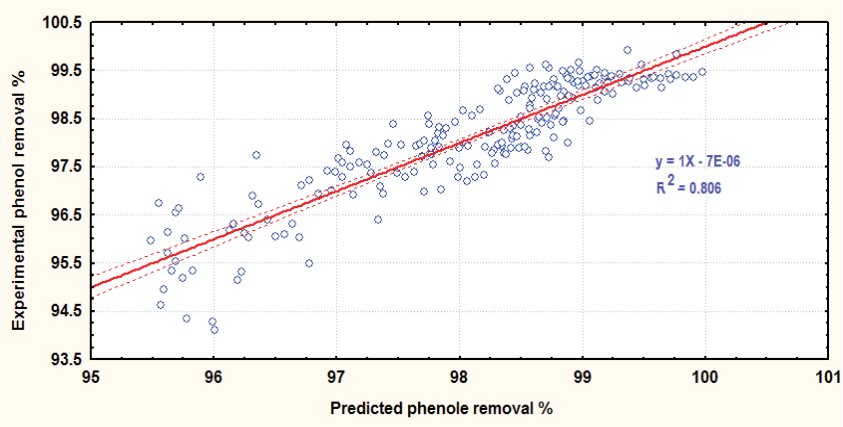

Fig. 10. Relationship between predicted and the experimental phenol removal by EC process at different operational conditions.

model that expresses the phenol adsorption. The kinetic feature of the phenol adsorption step was evaluated by using pseudo-first-order, pseudo-second-order, and intraparticle diffusion models. The presented data referred to the most favorability of the pseudo-second-order kinetics model, that is, it depends on both phenol and aluminum hydroxides' concentrations. The second step dealt with the complete dissociation of adsorbed phenol molecules to water and carbon dioxide gas. The complete phenol decomposition within 10 min of EC process was an economic technique with low energy consumption and TOC (0.75 US$/m^3). Accordingly, it seems advisable to use the EC technique as a fast, easy, economic, and safe technique in the full removal of phenol from its solutions. Interestingly, as it was accomplished in this study, the literature did not realize the complete decomposition of phenol into carbon dioxide and water in the solution, which was confirmed by analyses using various instruments.

References

[1] M. Kobya, E. Demirbas, O. Sahin, Effect of operational parameters on the removal of phenol from aqueous solutions by electrocoagulation using Fe and Al electrodes, Desal. Water Treat., 46 (2012) 366–374.
[2] E. Bazrafshan, H. Biglari, A.H. Mahvi, Phenol removal by electrocoagulation process from aqueous solutions, Fresenius Environ. Bull., 21 (2012) 364–371.
[3] U. Soni, J. Bajpai, S.K. Singh, A.K. Bajpai, Evaluation of chitosan-carbon based biocomposite for efficient removal of phenols from aqueous solutions, J. Water Process. Eng., 16 (2017) 56–63.
[4] O. Sahu, D.G. Rao, N. Gabbiye, A. Engidayehu, F. Teshale, Sorption of phenol from synthetic aqueous solution by activated saw dust: optimizing parameters with response surface methodology, Biochem. Biophys. Rep., 12 (2017) 46–53.
[5] W.W. Anku, M.A. Mamo, P.P. Govender, Chapter 17, Phenolic Compounds in Water: Sources, Reactivity, Toxicity and Treatment Methods, In: Phenolic Compounds-Natural Sources, Importance and Applications, In Tech., Open science, Open minds, 2017. Available at: http://dx.doi.org/10.5772/66927
[6] WHO, Guidelines for Drinking-Water Quality: Recommendations, World Health Organization, Geneva, 2004, pp. 540.
[7] E. Hernández-Francisco, J. Peral, L.M. Blanco-Jerez, Removal of phenolic compounds from oil refinery wastewater by electrocoagulation and Fenton/photo-Fenton processes, J. Water Process. Eng., 19 (2017) 96–100.
[8] R.R. Karri, N.S. Jayakumar, J.N. Sahu, Modelling of fluidised-bed reactor by differential evolution optimization for phenol removal using coconut shells based activated carbon, J. Mol. Liq., 231 (2017) 249–262.
[9] S.M. Nowee, M. Taherian, M. Salimi, S.M. Mousavi, Modeling and simulation of phenol removal from wastewater using a membrane contactor as a bioreactor, Appl. Math. Model., 42 (2017) 300–314.
[10] M. Caetano, C. Valderrama, A. Farran, J.L. Cortina, Phenol removal from aqueous solution by adsorption and ion exchange mechanisms onto polymeric resins, J. Colloid Interface Sci., 338 (2009) 402–409.
[11] S.A. Nor Aishah, J. Akhtar, H.K. Rai, Screening of combined zeolite-ozone system forphenol and COD removal, J. Chem. Eng., 158 (2010) 520–527.
[12] A. Ginos, T. Manios, D. Mantzavinos, Treatment of olive mill effluents by coagulation-flocculation-hydrogen peroxide oxidation and effect on phytotoxicity, J. Hazard. Mater., 133 (2006) 135–142.
[13] R. Sridar, U. Uma Ramanane, M. Rajasimman, ZnO nanoparticles – synthesis, characterization and its application for phenol removal from synthetic and pharmaceutical industry wastewater, Environ. Nanotechnol. Monit. Manage., 10 (2018) 388–393.
[14] B. Abussaud, H.A. Asmaly, T.A. Ihsanullah Saleh, V.K. Gupta, T. laoui, M.A. Atieh, Sorption of phenol from waters on activated carbon impregnated with iron oxide, aluminum oxide and titanium oxide, J. Mol. Liq., 213 (2016) 351–359.
[15] Z. Liu, H. Meng, H. Zhang, J. Cao, K. Zhou, J.M. Lian, Highly efficient degradation of phenol wastewater by microwave induced H_2O_2-CuOx/GAC catalytic oxidation process, Sep. Purif. Technol., 193 (2018) 49–57.
[16] I. Fatimah, E.Z. Pratiwi, W.P. Wicaksono, Synthesis of magnetic nanoparticles using *Parkia speciosa* Hassk pod extract and photocatalytic activity for Bromophenol blue degradation, EJAR, 46 (2020) 35–40.
[17] M.H.H. Ali, K.M. Al-Qahtani, S.M. El-Sayed, Enhancing photodegradation of 2,4,6 trichlorophenol and organic pollutants in industrial effluents using nanocomposite of TiO_2 doped with reduced graphene oxide, EJAR, 45 (2019) 321–328.
[18] M. Saleem, A.A. Bukhari, M.N. Akram, Electroco-agulation for the treatment of wastewater for reuse in irrigation and plantation, J. Basic Appl. Sci., 7 (2011) 11–20.
[19] E. Butler, Y.-T. Hung, Y.-L. Yeh, M.S. Al Ahmad, Electrocoagulation in wastewater treatment, Water, 3 (2011) 495–525.
[20] G. Mouedhen, M. Feki, M.W. De Petris, H.F. Ayedi, Behavior of aluminum electrodes in electrocoagulation process, J. Hazard. Mater., 150 (2008) 124–135.

[21] M. Uğurlu, A. Gürses, Ç. Doğar, M. Yalçın, The removal of lignin and phenol from paper mill effluents by electrocoagulation, J. Environ. Manage., 87 (2008) 420–428.
[22] M.A. Zazouli, M. Taghavi, Phenol removal from aqueous solutions by electrocoagulation technology using iron electrodes: effect of some variables, J. Water Resour. Prot., 4 (2012) 980–983.
[23] A.S. Fajardo, R.F. Rodrigues, R.C. Martins, L.M. Castro, R.M. Quinta-Ferreira, Phenolic wastewaters treatment by electrocoagulation process using Zn anode, J. Chem. Eng., 275 (2015) 331–341.
[24] A.A. Moneer, M.M. El-Sadaawy, G.F. El-Said, F.A.M. Morsy, Modeling adsorption kinetic of crystal violet removal by electrocoagulation technique using bipolar ironelectrodes, Water Sci. Technol., 77 (2018) 323–336.
[25] O.T. Can, M. Bayramoglu, M. Kobya, Decolorization of reactive dye solutions by electrocoagulation using aluminum, Ind. Eng. Chem. Res., 42 (2003) 3391–3396.
[26] A.M. Shaker, A.A. Moneer, M.M. El-Sadaawy, N.M. El-Mallah, M.SH. Ramadan, Comparative study for removal of acid green 20 dye by electrocoagulation technique using aluminum and iron electrodes, Desal. Water Treat., 198 (2020) 345–363.
[27] APHA, Standard Methods for the Examination of Water and Wastewater, 20th ed., APHA/AWWA/WEF, Washington, DC, 1998.
[28] O. Abdelwahab, N.K. Amin, E.-S.Z. El-Ashtoukhy, Electrochemical removal of phenol from oil refinery wastewater, J. Hazard. Mater., 163 (2009) 711–716.
[29] M.A. Zazouli, M. Taghavi, E. Bazrafshan, Influences of solution chemistry on phenol removal from aqueous environments by electrocoagulation process using aluminum electrodes, J. Health Scope, 1 (2012) 66–70.
[30] Z. Wu, M. Zhou, Partial degradation of phenol by advanced electrochemical oxidation process, Environ. Sci. Technol., 35 (2001) 2698–2703.
[31] X.-Y. Li, Y.-H. Cui, Y.-J. Feng, Z.-M. Xie, J.-D. Gu, Reaction pathways and mechanisms of the electrochemical degradation of phenol on different electrodes, Water Res., 39 (2005) 1972–1981.
[32] A.A. Mohammed, Electrocoagulation of phenol for wastewater treatment, Iraqi J. Chem. Petrol. Eng., 9 (2007) 37–41.
[33] M. Saravanan, N.P. Sambhamurthy, M. Sivarajan, Treatment of acid blue 113 dye solution using iron electrocoagulation, Clean Soil Air Water, 38 (2010) 565–571.
[34] M.M. Naim, A.A. Moneer, G.F. El-Said, Predictive equations for the defluoridation by electrocoagulation technique using bipolar aluminum electrodes in the absence and presence of additives: a multivariate study, Desal. Water Treat., 57 (2016) 6320–6332.
[35] N. Modirshahla, M.A. Behnajady, S. Mohammadi-Aghdam, Investigation of the effect of different electrodes and their connections on the removal efficiency of 4-nitrophenol from aqueous solution by electrocoagulation, J. Hazard. Mater., 154 (2008) 778–786.
[36] N. Modirshahla, M.A. Behnajady, S. Kooshaiian, Investigation of the effect of different electrodes connections on the removal efficiency of Tartrazine from aqueous solutions by electrocoagulation, Dyes Pigm., 74 (2007) 249–257.
[37] R. Kamaraj, P. Ganesan, J. Lakshmi, S. Vasudevan, Removal of copper from water by electrocoagulation process-effect of alternating current (AC) and direct current (DC), Environ. Sci. Pollut. Res., 20 (2013) 399–412.
[38] G. Piotrowska, B. Pierozynski, Electrodegradation of phenol through continuous electrolysis of synthetic wastewater on platinized titanium and stainless-steel anodes, Int. J. Electrochem. Sci., 12 (2017) 4444–4455.
[39] B. Pierozynski, G. Piotrowska, Electrochemical degradation of phenol and resorcinol molecules through the dissolution of sacrificial anodes of macro-corrosion galvanic Cells, Water, 10 (2018) 770. doi: 10.3390/w10060770.
[40] S. Vasudevan, An efficient removal of phenol from water by peroxi- ectrocoagulation processes, J. Water Process. Eng., 2 (2014) 53–57.
[41] M.H. Umberit, A. Jędrasiewicz, Application of infrared spectrophotometry to the identification of inorganic substances in dosage forms of antacida group, Acta Poloniac Pharmaceutica – Drug Res., 57 (2000) 83–91.
[42] Y.J.O. Asencios, M.R. Sun-Kou, Synthesis of high-surface-area γ-Al_2O_3 from aluminum scrap and its use for the adsorption of metals: Pb(II), Cd(II) and Zn(II), Appl. Surf. Sci., 258 (2012) 10002–10011.
[43] M. Pimentel, N. Oturan, M. Dezotti, M.A. Oturan, Phenol degradation by advanced electrochemical oxidation process electro-Fenton using a carbon felt cathode, Appl. Catal. B, 83 (2008) 140–149.
[44] S. Vasudevan, J. Lakshmi, G. Sozhan, Optimization of electrocoagulation process for the simultaneous removal of mercury, lead, and nickel from contaminated water, Environ. Sci. Pollut. Res., 19 (2012) 2734–2744.
[45] F. Liu, K. Zhou, Q. Chen, A. Wang, W. Chen, Application of magnetic ferrite nanoparticles for removal of Cu(II) from copper-ammonia wastewater, J. Alloys Compd., 773 (2019) 140–149.
[46] A.H. Shobier, M.M. El-Sadaawy, G.F. El-Said, Removal of hexavalent chromium by ecofriendly raw marine green alga *Ulva fasciata:* kinetic, thermodynamic and isotherm studies, EJAR, in press (2020) https://doi.org/10.1016/j.ejar.2020.09.003.
[47] R. Kamaraj, S. Vasudevan, Facile one-pot synthesis of nano-zinc hydroxide by electro-dissolution of zinc as a sacrificial anode and the application for adsorption of Th^{4+}, U^{4+}, and Ce^{4+} from aqueous solution, Res. Chem. Intermed., 42 (2016) 4077–4095.
[48] A. Gouthaman, R.S. Azarudeen, A. Gnanaprakasam, V.M. Sivakumar, M. Thirumarimurugan, Polymeric nanocomposites for the removal of Acid red 52 dye from aqueous solutions: synthesis, characterization, kinetic and isotherm studies, Ecotoxicol. Environ. Saf., 160 (2018) 42–51.
[49] S. Vasudevan, J. Lakshmi, G. Sozhan, Electrocoagulation studies on the removal of copper from water using mild steel electrode, Water Environ. Res., 84 (2012) 209–219.
[50] R. Kamaraj, A. Pandiarajan, S. Jayakiruba, Mu. Naushad, S. Vasudevan, Kinetics, thermodynamics and isotherm modeling for removal of nitrate from liquids by facile one-pot electrosynthesized nano zinc hydroxide, J. Mol. Liq., 215 (2016) 204–211.
[51] G.F. El-Said, M.M. El-Sadaawy, M.A. Aly-Eldeen, Adsorption isotherms and kinetic studies for the defluoridation from aqueous solution using eco-friendly raw marine green algae, *Ulva lactuca*, Environ. Monit. Assess., 190 (2018) 14.
[52] A. Pholosi, E.B. Naidoo, A.E. Ofomaja, Intraparticle diffusion of Cr(VI) through biomass and magnetite coated biomass: a comparative kinetic and diffusion study, S. Afr. J. Chem. Eng., 32 (2020) 39–55.
[53] D. Núñez-Gómeza, C. Rodriguesa, F.R. Lapollia, M.Á. Lobo-Recio, Adsorption of heavy metals from coal acid mine drainage by shrimp shell waste: isotherm and continuous-flow studies, J. Environ. Chem. Eng., 7 (2019) 102787.
[54] K. Rambabu, G. Bharatha, F. Banat, P.L. Show, Biosorption performance of date palm empty fruit bunch wastes for toxic hexavalent chromium removal, Environ. Res., 187 (2020) 109694.
[55] M.I. Jalees, M.U. Farooq, S. Basheer, S. Asghar, Removal of heavy metals from drinking water using chikni mitti (kaolinite): isotherm and kinetics, Arab. J. Sci. Eng., 44 (2019) 6351–6359.
[56] W.J. Weber Jr, J.C. Morriss, Kinetics of adsorption on carbon from solution, J. Sanit. Eng. Div., 89 (1963) 31–60.
[57] B.N. Patil, D.B. Nalk, S. Shrivastava, Photocatalytic degradation of hazardous ponceau-S dye from industrial wastewater, Desalination, 269 (2011) 276–283.
[58] F.I. El-Hosiny, M.A. Abdel-Khalek, K.A. Selim, I. Osama, Physicochemical study of dye removal using electrocoagulation flotation process, Physicochem. Probl. Mineral Process., 54 (2018) 321–333.
[59] M. Kobya, E. Gengec, E. Demirbas, Operating parameters and costs assessments of a real dyehouse wastewater effluent treated by a continuous electrocoagulation process, Chem. Eng. Process., 101 (2016) 87–100.